Hyperbolic Conservation Laws on 3D Cubed-Sphere Grids: A Parallel High-Order Solution-Adaptive Simulation Framework

Prof. Hans De Sterck

Scalable Scientific Computing Group
Applied Mathematics University of Waterloo

CAIMS, Toronto, June 26, 2012

Co-authors

University of Waterloo
Scalable Scientific Computing Group

- **Dr. Lucian Ivan,** Postdoctoral Fellow
- **Andree Susanto**, Ph.D. Candidate

University of Toronto Institute for Aerospace Studies (UTIAS)
CFD and Propulsion Group

- **Prof. Clinton Groth**
- **Scott Northrup**, Ph.D. Candidate and Parallel Programming Analyst at SciNet

CSA Canadian Geospace Monitoring (CGSM) Program

Project: **"Solar Drivers of Space Weather: Contributions to Forecasting"**

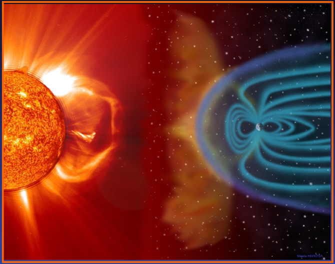

Goal: Develop advanced simulation methods for MHD space plasmas and apply to space-weather forecasting.

Housed At: Applied Math., U. Waterloo

Collaborators: UTIAS, NRCan, Others

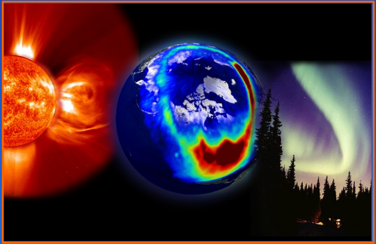

Images courtesy of SOHO/EIT consortium

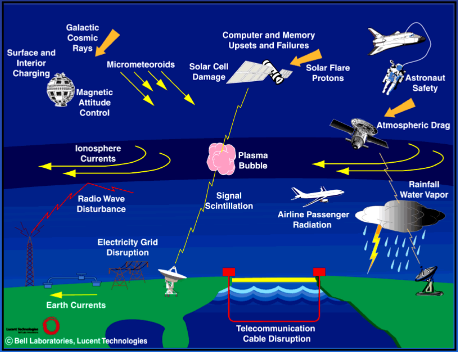

Image courtesy of NASA

3D Gnomonic Cubed-Sphere Grids

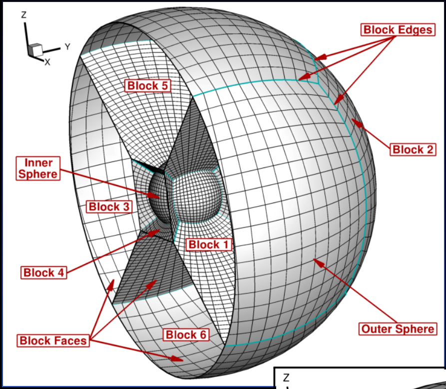

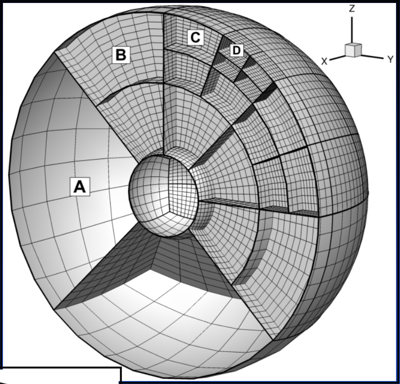

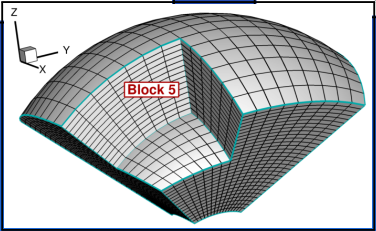

Potential Benefits of High-Order AMR Approaches

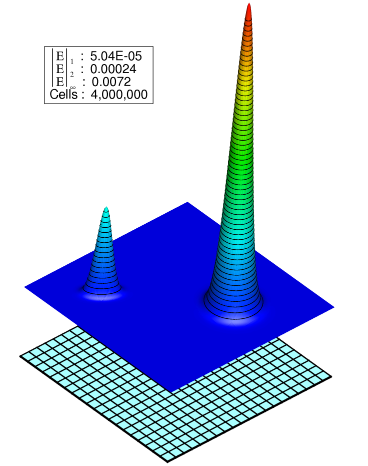

Linear reconstruction on uniform mesh

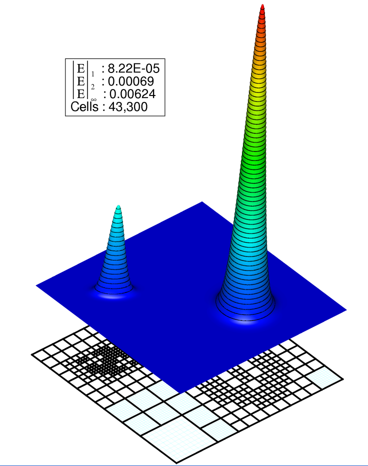

Cubic reconstruction with AMR

Talk Outline

1. Governing Equations
2. Parallel Implicit Solution-Adaptive Cubed-Sphere Simulation Framework
3. Extension to High-Order Accuracy
4. Numerical Results
5. Concluding Remarks & Future Research

Ideal Magnetohydrodynamics (MHD) Equations

Flow Governed by 3D Compressible MHD Equations

- perfectly-conducting single-species fluid, isotropic pressure, magnetized inviscid compressible perfect gas (i.e. $p = \rho RT$)

$$\frac{\partial}{\partial t}\left|\begin{array}{c}\rho \\ \rho\vec{V} \\ \vec{B} \\ \rho e\end{array}\right| + \vec{\nabla}\cdot\left|\begin{array}{c}\rho\vec{V} \\ \rho\vec{V}\vec{V} + (p + \vec{B}\cdot\vec{B}/2)\vec{\vec{I}} - \vec{B}\vec{B} \\ \vec{V}\vec{B} - \vec{B}\vec{V} \\ (\rho e + p + \vec{B}\cdot\vec{B}/2)\vec{V} - (\vec{V}\cdot\vec{B})\vec{B}\end{array}\right| = \mathbf{Q} + \mathbf{S}$$

$$\frac{\partial \mathbf{U}}{\partial t} + \vec{\nabla}\cdot\vec{\mathbf{F}} = \mathbf{Q} + \mathbf{S}, \qquad \nabla\cdot\vec{B} = 0$$

Main Challenges to the Numerical Discretization

- Maintain physical solution (e.g. positive pressure & density)
- Provide both solution accuracy and monotonicity even in the presence of discontinuous solutions (e.g. shocks, contacts)
- Avoid shockwave instabilities (e.g. carbuncle phenomenon)

Ideal Magnetohydrodynamics (MHD) Equations

Approaches to Deal with the Divergence Constraint Condition, $\nabla \cdot \vec{B} = 0$

Powell Source Term (Powell *et. al.*, 1999)

$$\mathbf{S} = -\nabla \cdot \vec{B} \left[\; 0, \;\; \vec{B}, \;\; \vec{V}, \;\; \vec{V} \cdot \vec{B} \; \right]^{\mathrm{T}}$$

- 8-wave MHD system that is symmetric and Galilean invariant
  $\lambda_{1,2} = v_x \pm c_{fx}, \;\; \lambda_{3,4} = v_x \pm c_{Ax}, \;\; \lambda_{5,6} = v_x \pm c_{sx}, \;\; \lambda_{7,8} = v_x$
- Numerical error in $\nabla \cdot \vec{B}$ is convected out of the domain by $\lambda_8 = v_x$

Divergence Correction Technique: Generalized Lagrange Multiplier (GLM)-MHD (Dedner *et al.*, 2002)

$$\frac{\partial \vec{B}}{\partial t} + \nabla \cdot (\vec{V}\vec{B} - \vec{B}\vec{V}) + \nabla \psi = 0$$

$$\frac{\partial \psi}{\partial t} + c_h^2 \nabla \cdot \vec{B} = -\frac{c_h^2}{c_p^2} \psi$$

- Solve an extra transport equation for the GLM, ψ
- $\lambda_{8,9} = \pm c_h$, the largest eigenvalue in the domain

Talk Outline

1. Governing Equations
2. Parallel Implicit Solution-Adaptive Cubed-Sphere Simulation Framework
3. Extension to High-Order Accuracy
4. Numerical Results
5. Concluding Remarks & Future Research

Discretizations of Spherical Domains

Several Options in the Literature

- Latitude-longitude grid constructs

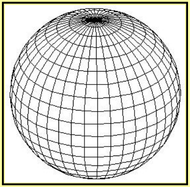

- Cubed sphere

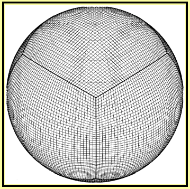

- Cartesian cut-cell approach

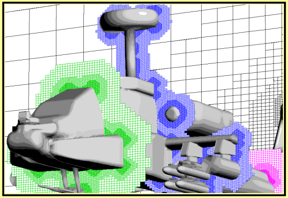

- Geodesic grid (e.g. icosahedron)

3D Cubed-Sphere Multi-Block Mesh in CFFC

Adequate Data Structured Required to Handle the Complex Block Connectivity

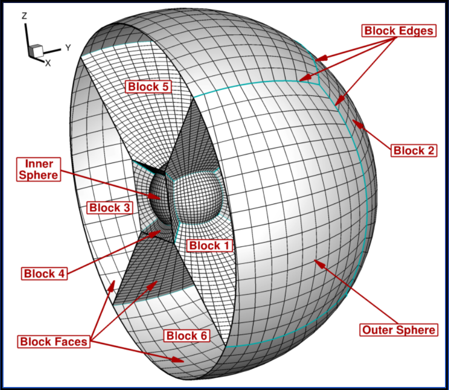

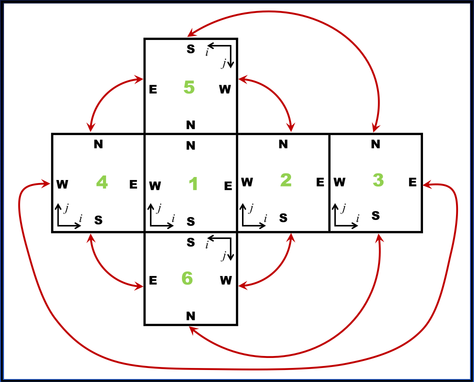

Cross-section of the cubed-sphere grid (**left)** and illustration of connectivity among blocks (**right)**

Computational Elements (Cells, Control Volumes)

Accurate Geometry Representation Required for High-Order Schemes

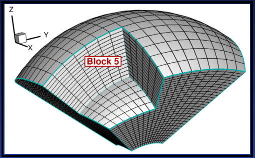

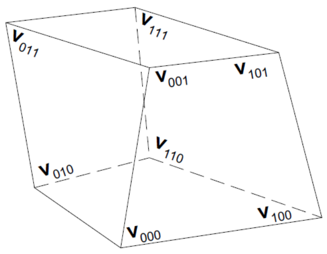

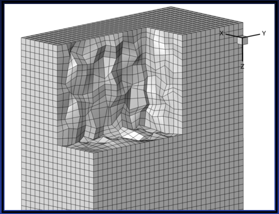

Representative hexa for 3D cubed-sphere grids

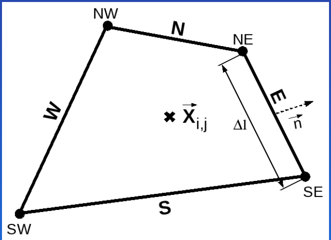

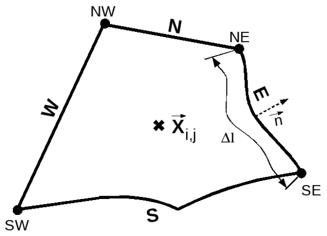

Examples of 2D quadrilaterals with straight and curved edges

Parallel Implicit AMR Finite-Volume Framework

Finite-Volume Formulation

General System of Conservation Laws

$$\frac{\partial \mathbf{U}}{\partial t} + \vec{\nabla} \cdot \vec{\mathbf{F}} = \mathbf{S} + \mathbf{Q}$$

Semi-Discrete Integral Form for Hexahedral Cell (i,j,k)

$$\frac{d\overline{\mathbf{U}}_{i,j,k}}{dt} = -\frac{1}{V_{i,j,k}} \sum_{m=1}^{N_f} \left(\vec{\mathbf{F}} \cdot \vec{n}\, \Delta A\right)_{i,j,k,m} + \left(\overline{\mathbf{S}}\right)_{i,j,k} + \left(\overline{\mathbf{Q}}\right)_{i,j,k} = \mathbf{R}_{i,j,k}(\overline{\mathbf{U}})$$

Primary Steps to Obtaining Numerical Solution

- **Solution reconstruction**: limited piecewise linear approximation
- **Spatial residual computation**:
  - Interface flux evaluation: hyperbolic (& elliptic fluxes)
  - Source term integration
- **Time Integration**: evolve solution forward in time
  - Multi-stage explicit time marching schemes (e.g., RK2, RK4)
  - Parallel implicit NKS algorithm (Northrup & Groth, 2009)

Parallel Implicit AMR Finite-Volume Framework

Linear Least-Squares Reconstruction (Barth, 1993) on Cubed-Sphere Grids

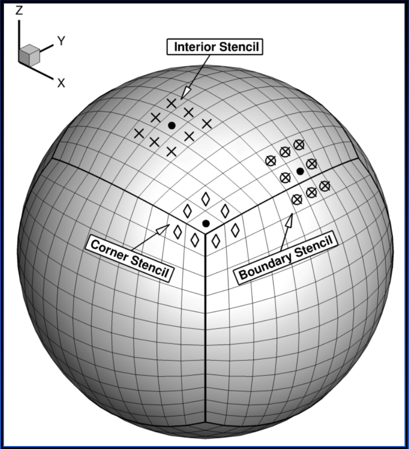

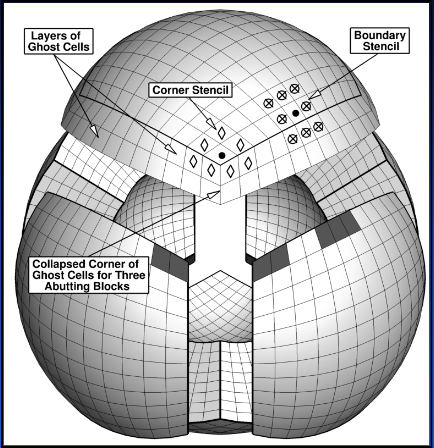

Linear Reconstruction of Primitive Variables

$$\mathbf{W}_{i,j,k}(\vec{x}) = \overline{\mathbf{W}}_{i,j,k} + \Phi_{i,j,k} \vec{\nabla}\mathbf{W} \cdot (\vec{x} - \vec{x}_{i,j,k})$$

Numerical Flux Evaluation for Calculating $\mathbf{R}_{i,j,k}(\overline{\mathbf{U}})$

- Solve a Riemann problem at each integration point to provide **upwinding**

$$\vec{\mathbf{F}}_{\mathrm{H}} = \vec{\mathcal{F}}_{\mathrm{H}}\left(\mathbf{U}_{\mathrm{L}}, \mathbf{U}_{\mathrm{R}}, \vec{n}\right) = \frac{1}{2}\left(\vec{\mathbf{F}}_{\mathrm{H}}\left(\mathbf{U}_{\mathrm{R}}, \vec{n}\right) + \vec{\mathbf{F}}_{\mathrm{H}}\left(\mathbf{U}_{\mathrm{L}}, \vec{n}\right)\right) - \frac{1}{2}\left|A\left(\mathbf{U}_{\mathrm{R}}, \mathbf{U}_{\mathrm{L}}, \vec{n}\right)\right|\left(\mathbf{U}_{\mathrm{R}} - \mathbf{U}_{\mathrm{L}}\right)$$

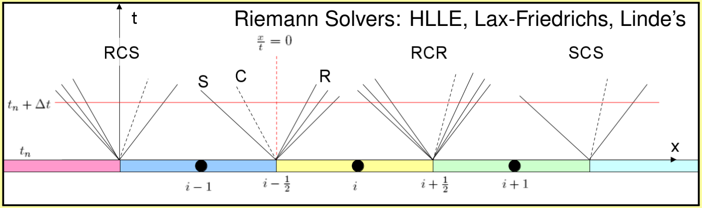

- Some Riemann solvers use only the fastest and slowest waves
- There are six flux evaluation points for a hexahedral cell

Inexact Newton's Method

- Semi-discrete form of the governing equations for steady flows

$$\mathbf{R}(\mathbf{U}) = 0 \tag{1}$$

- Apply Newton's method to solve Eq. (1) for $\mathbf{U}$

$$\left(\frac{\partial \mathbf{R}}{\partial \mathbf{U}}\right)^n \Delta \mathbf{U}^n = \mathbf{J}^n \Delta \mathbf{U}^n = -\mathbf{R}(\mathbf{U}^n) \tag{2}$$

$$\mathbf{U}^{n+1} = \mathbf{U}^n + \Delta \mathbf{U}^n$$

- Solve at each Newton step the sparse linear system of Eq. (2)

$$\mathbf{J}\mathbf{x} = \mathbf{b}$$

  using a preconditioned iterative linear solver (GMRES) which is not fully converged

Parallel Implicit AMR Finite-Volume Framework

Mechanics of Block-Based AMR (Simple 2D Example)

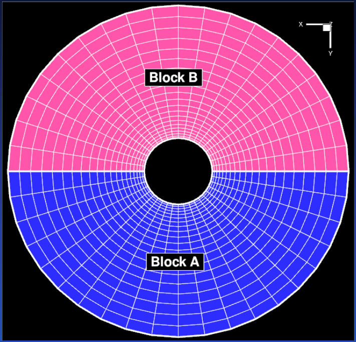

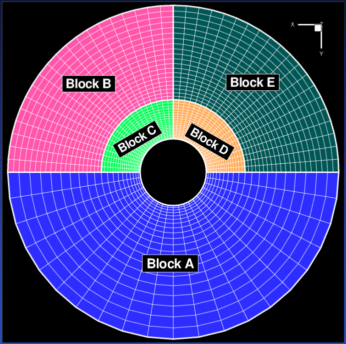

- Berger (1984); Berger & Colella (1989); Quirk (1991); De Zeeuw & Powell (1993); Quirk & Hanebutte (1993); Berger & Saltzman (1994); Groth *et al.* (1999, 2000); Keppens *et al.* (2011)
- AMR algorithm for multi-block body-fitted mesh: Sachdev *et al.* (2005); Northrup & Groth (2005); Gao & Groth (2008, 2010); Ivan & Groth (2007, 2011)

Parallel Implicit AMR Finite-Volume Framework

3D Block-Based AMR (Berger, 1984; Gao & Groth, 2010)

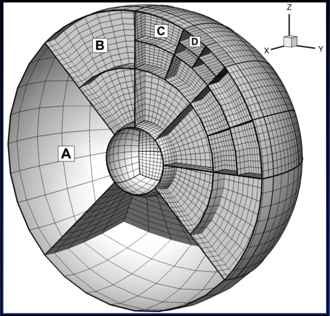

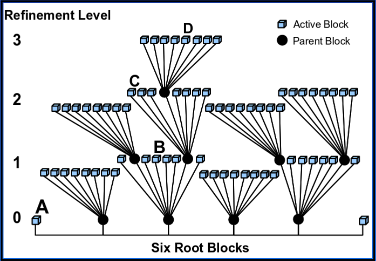

- Mesh refinement by division and coarsening of self-similar structured blocks (hexahedral cells)
- Solution transfer among blocks via overlapping ghost cells
- Hierarchical octree data structure provides block connectivity
- Permits local refinement of mesh
- Physics-based refinement criteria (e.g. $\epsilon_1 \propto |\vec{\nabla}\rho|$, $\epsilon_2 \propto |\vec{\nabla}\cdot\vec{V}|$, $\epsilon_3 \propto |\vec{\nabla}\otimes\vec{V}|$)
- Permits parallel implementation via domain decomposition
- Highly efficient load balancing is obtained by equally distributing the solution blocks among CPUs

Parallel Implicit AMR Finite-Volume Framework

3D AMR on Cubed-Sphere Grid

CFFC Implementation

- Truly 3D AMR (also used as block-multiplication procedure)
- Body-fitted mesh by constraining the points on the boundary spheres

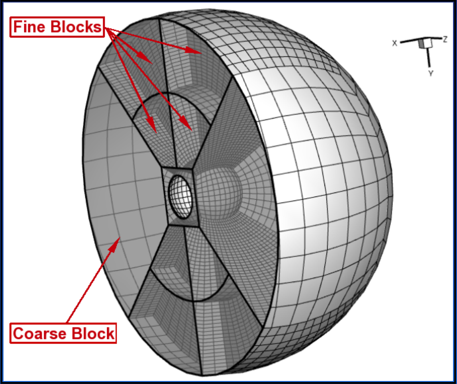

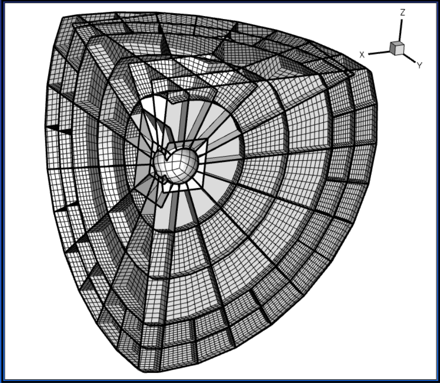

Parallel Implicit AMR Finite-Volume Framework

Transparent Reconstruction for Blocks of Different Resolution

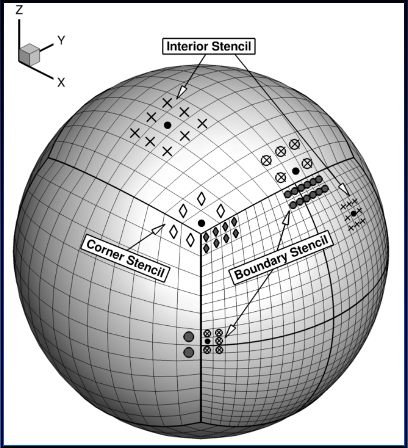

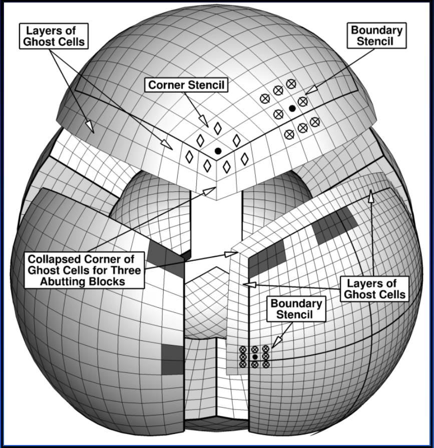

Linear Reconstruction of Primitive Variables

$$\mathbf{W}_{i,j,k}(\vec{x}) = \overline{\mathbf{W}}_{i,j,k} + \Phi_{i,j,k}\vec{\nabla}\mathbf{W}\cdot(\vec{x}-\vec{x}_{i,j,k})$$

Transparent Implementation At Block Boundaries

Goals: Have Transparency At Block Boundaries For

- high-order accurate fluxes
- adaptivity
- implicit time integration
- parallelisation

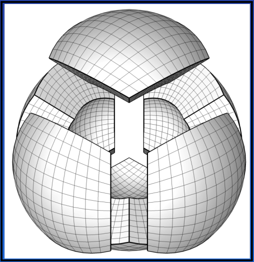

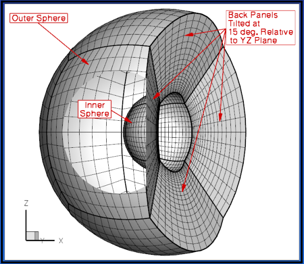

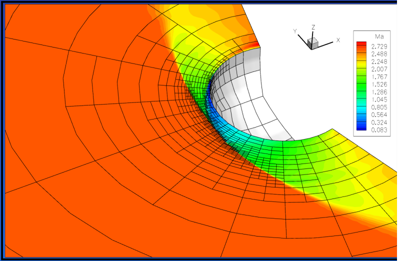

Transparent Implementation At Block Boundaries

Technical Details

- unstructured root block connectivity
- consistently keep track of (i, j, k) orientation ordering
- k-exact least-squares with variable stencil size
- collapsed ghost cells at degenerated corners
- limit mesh resolution change to factor 2
- parallel domain decomposition with self-similar soln. blocks

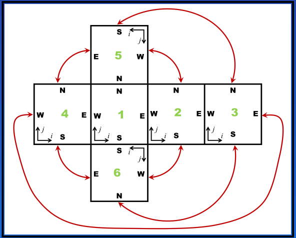

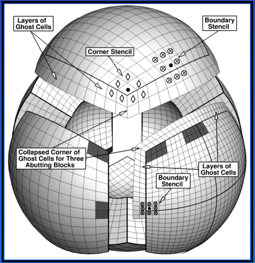

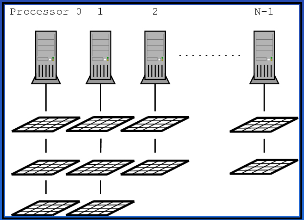

Talk Outline

1. Governing Equations
2. Parallel Implicit Solution-Adaptive Cubed-Sphere Simulation Framework
3. Extension to High-Order Accuracy
4. Numerical Results
5. Concluding Remarks & Future Research

Extension to High-Order Accuracy

Overview Idea of the High-Order MHD Algorithm

- Apply a high-order **CENO** approach (Ivan & Groth, 2007) (initially proposed for 2D inviscid and viscous flows, but not for MHD)
- Use CENO + GLM-MHD (Dedner *et al.*, 2002) to satisfy $\nabla \cdot \vec{B} = 0$

Central Essentially Non-Oscillatory (CENO) Idea

- ENO Property: **Spurious oscillations** proportional to the size of the jump at points of discontinuity **are NOT allowed** (i.e. no Gibbs-like phenomenon) but **they may exist** on the **order of truncation error**.
- Combine an unlimited k-exact reconstruction with a monotonicity preserving limited linear $(k=1)$ scheme
- Use a single (central) stencil for reconstruction
- Hybrid method: use a smoothness indicator to switch between reconstruction procedures

Note: ENO scheme on a fixed central stencil have been explored in 1D by Harten & Chakravarthy, 1991

CENO High-Order Finite-Volume Formulation

2D Algorithm on Quadrilateral Elements

General System of Conservation Laws

$$\frac{\partial \mathbf{U}}{\partial t} + \vec{\nabla} \cdot \vec{\mathbf{F}} = \mathbf{S} + \mathbf{Q}$$

Semi-Discrete Integral Form for Quadrilateral Element

$$\frac{d\overline{\mathbf{U}}_{i,j}}{dt} = -\frac{1}{A_{i,j}} \oint_{\Omega} \vec{\mathbf{F}} \cdot \vec{n}\, d\ell + \frac{1}{A_{i,j}} \iint_{\mathcal{A}} (\mathbf{S} + \mathbf{Q})\, da = \mathbf{R}_{i,j}(\overline{\mathbf{U}})$$

Primary Steps to Obtaining Numerical Solution

- **Solution reconstruction**: high-order piecewise polynomials
- **High-order spatial residual computation**:
  - Interface flux evaluation: hyperbolic & elliptic fluxes
  - Source term integration
- **Time Integration**: evolve solution forward in time
  - Multi-stage explicit time marching schemes (e.g., RK2, RK4)

CENO High-Order Finite-Volume Formulation

High-Order Spatial Discretization Procedure

Requires More Accurate Evaluation of $\mathbf{R}_{i,j}(\overline{\mathbf{U}})$

- **More accurate calculation of flux and source term integrals**

$$\frac{1}{A_{i,j}} \oint_{\Omega} \vec{\mathbf{F}} \cdot \vec{n}\, d\ell = \frac{1}{A_{i,j}} \sum_{l=1}^{N_f} \sum_{m=1}^{N_G} \left(\omega \vec{\mathbf{F}} \cdot \vec{n}\, \Delta\ell \right)_{i,j,l,m}$$

  - **Solution** $\Rightarrow$ Use more Gauss quadrature points ($N_G \geq 2$)

- **More accurate numerical flux at each integration point**

  Upwinding **hyperbolic flux** by solving a Riemann problem

$$\vec{\mathbf{F}}_{\mathrm{H}} = \vec{\mathcal{F}}_{\mathrm{H}} \left(\mathbf{U}_{\mathrm{L}}, \mathbf{U}_{\mathrm{R}}, \vec{n} \right)$$

  - **Solution** $\Rightarrow$ Evaluate $\mathbf{U}$ more accurately at faces of computational cells (i.e., high-order solution reconstruction)

Central ENO (CENO) Reconstruction in 3D

- Piecewise polynomial approximation for solution:

$$W^k_{i,j,\kappa}(\vec{r}) = \sum_{p_1=0}^{k} \sum_{p_2=0}^{k} \sum_{\substack{p_3=0 \\ (p_1+p_2+p_3\le k)}}^{k} (x-\bar{x}_{i,j,\kappa})^{p_1} (y-\bar{y}_{i,j,\kappa})^{p_2} (z-\bar{z}_{i,j,\kappa})^{p_3} D^k_{p_1p_2p_3}$$

- Use a trilinear interpolation to represent skewed hexas accurately
- Compute all volume and face integrals based on the trilinear mapping
- Use a supporting stencil to determine $D_{p_1p_2p_3}$ (e.g., maximum 125 cells for cubic and quartic polynomials)

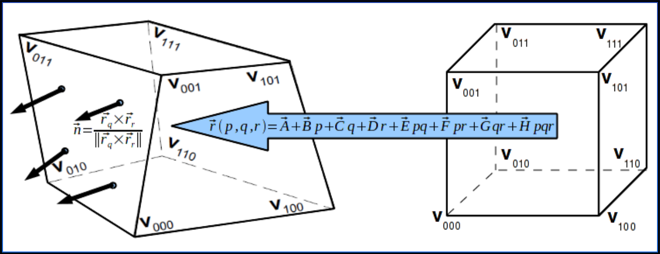

Talk Outline

1. Governing Equations
2. Parallel Implicit Solution-Adaptive Cubed-Sphere Simulation Framework
3. Extension to High-Order Accuracy
4. **Numerical Results**
5. Concluding Remarks & Future Research

Numerical Results in 2D

Supersonic Flow Past Cylinder at $M_\infty = 2.1$ **Final mesh: 2,150 10×10 blocks**

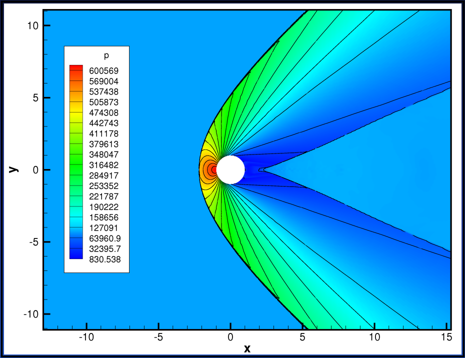

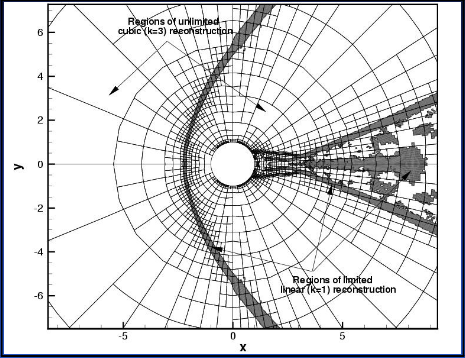

Predicted pressure distribution obtained using the **4th-order CENO** scheme on final refined AMR mesh and regions of limited and unlimited reconstruction

Numerical Results in 2D

Superfast Rotating Outflow from the Cylinder

$R_i = 1$, $R_o = 6$, **Inflow:** $\rho = 1$, $p = 1$, $V_r = 3$, $V_\theta = 1$, $B_r = 1$

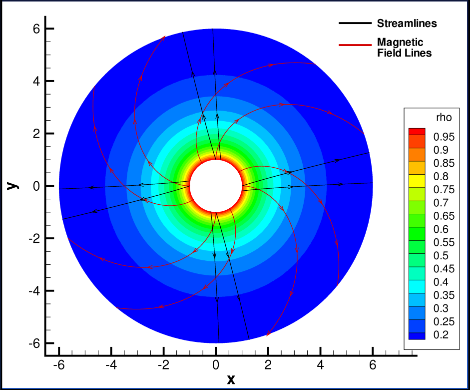

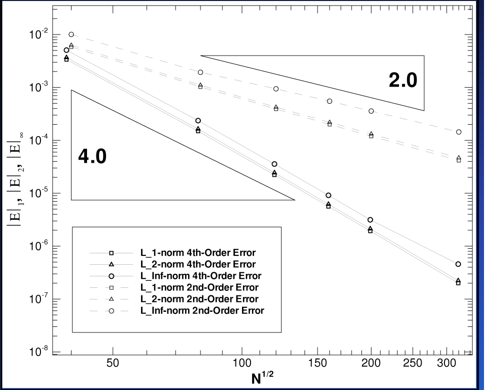

Predicted density distribution obtained using the **4th-order CENO** scheme with GLM-MHD on a 80×80 mesh (left).
Error norms in the predicted solution entropy (right).

Numerical Results in 2D

MHD Shu-Osher's Shock Tube at 45° Relative to Grid
Interaction of sinusoidal density variation with moving shockwave

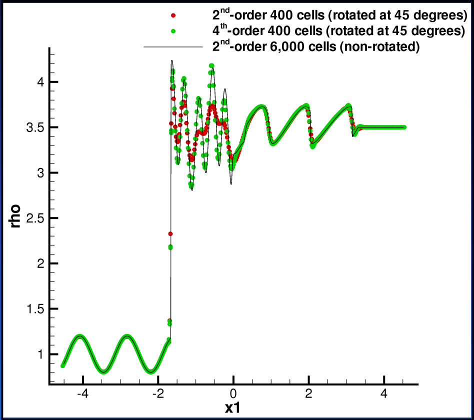

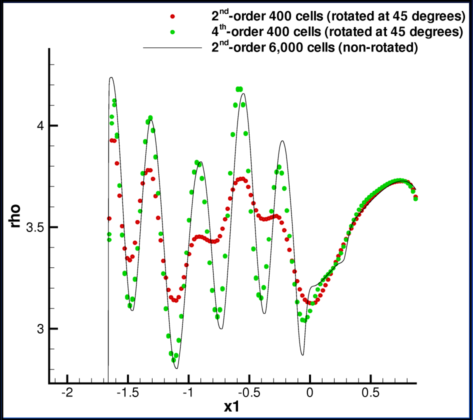

Comparison of predicted density distributions obtained using the **4th-order CENO** and the **2nd-order** schemes in combination with GLM-MHD.

Numerical Results in 3D

Transonic Wind on AMR Mesh $R_i = 1$, $R_o = 10$, $GM_* = 14$, **Inflow:** $\rho = 5$, $p = 23$

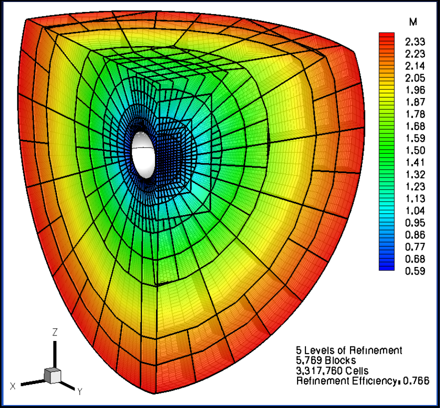

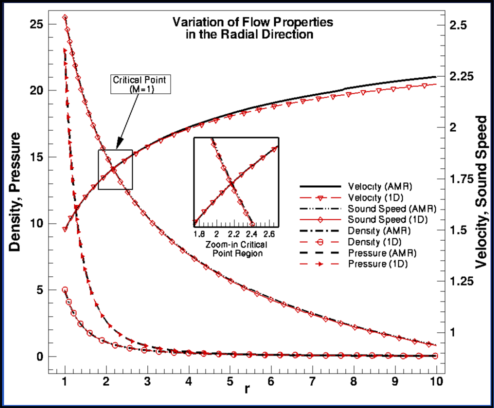

Predicted Mach number distribution obtained on the adapted cubed-sphere mesh (left). Comparison of flow properties in the X-axis direction relative to a highly-accurate 1D “exact solution” (right).

Numerical Results in 3D

Time-Invariant Solar Wind $R_i = 1$, $R_o = 100$, $\gamma = 5/3$, $n_s = 1.4\times10^8\text{cm}^{-3}$, $T_s = 2.0\times10^6\text{K}$

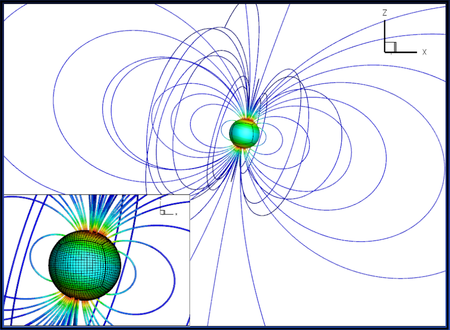

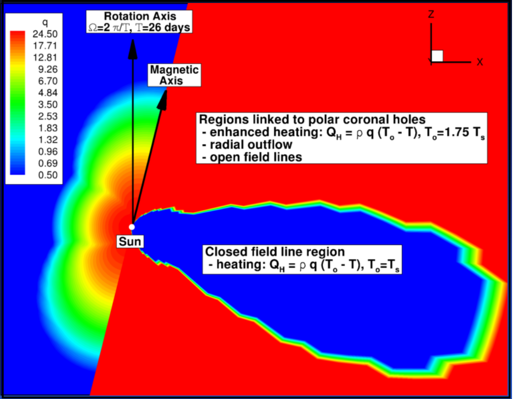

Solar wind conditions based on the model of Groth *et al.*, 2000

- Magnetic field strength: 8.4 G at the poles and 2.2 G at the equator.
- Differential heating in closed and open field line regions
- The actual simulation had the magnetic and rotational axes aligned.

Numerical Results in 3D

Time-Invariant Solar Wind $R_i = 1$, $R_o = 30$, $\gamma = 5/3$, $n_s = 1.4 \times 10^8 \text{cm}^{-3}$, $T_s = 2.0 \times 10^6 \text{K}$

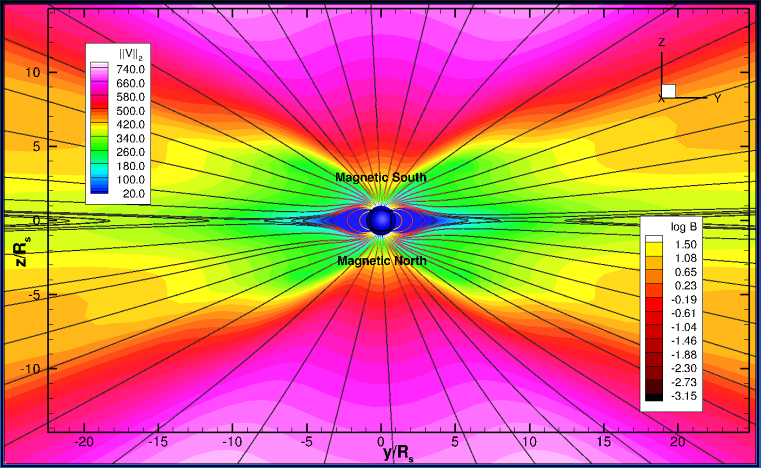

Prediction of solar-wind speed and magnitude of $\vec{B}$ obtained on 96 $20 \times 20 \times 20$ blocks and 768,000 cells.

Numerical Results in 3D

Time-Invariant Solar Wind $R_i = 1$, $R_o = 30$, $\gamma = 5/3$, $n_s = 1.4 \times 10^8 \mathrm{cm}^{-3}$, $T_s = 2.0 \times 10^6 \mathrm{K}$

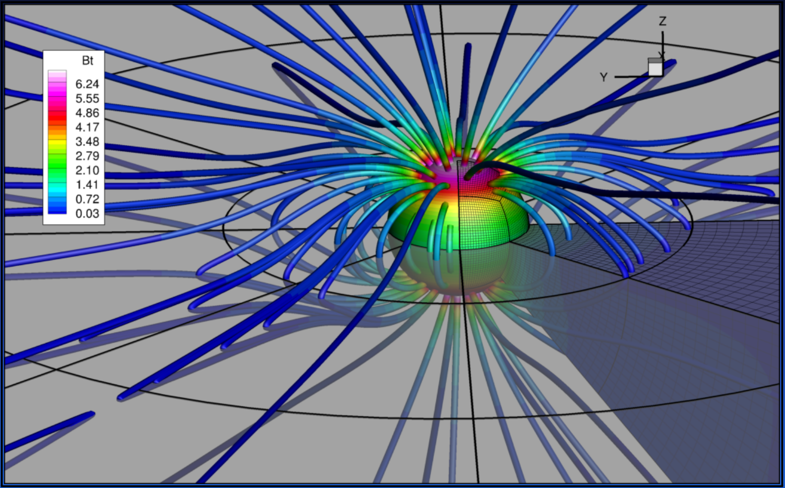

Close-up view of magnetic field lines and multi-block mesh

Numerical Results in 3D

CFFC Parallel Strong Scaling Performance on SciNet GPC (Nehalem processors)

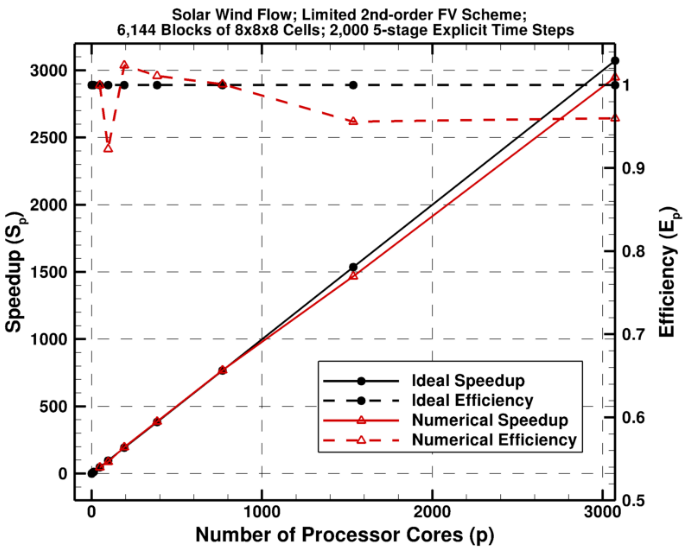

Numerical Results in 3D

Reconstruction of $f(x,y,z) = (\cos(\pi(y+1)) - \cos(\pi z))e^{-\pi(x+1)}$ on Distorted Meshes

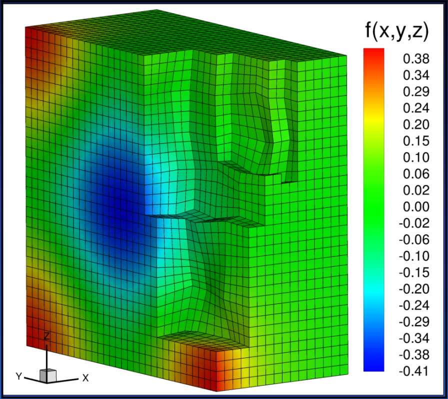

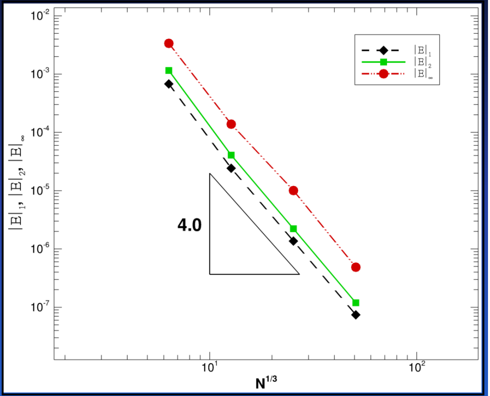

Solution reconstruction obtained using the **4th-order CENO** scheme on a mesh with 8 blocks of $4\times8\times8$ and 2,048 cells (left) and error norms (right).

Numerical Results in 3D

Magnetohydrostatic Test Case on Cartesian Box (Warburton 1999)

$$\mathbf{U}(x,y,z)=\left[1,\vec{0},\,(\cos(\pi(y+1))-\cos(\pi z))f(x),\,\cos(\pi z)f(y)+\sin(\pi(y+1))f(x),\,\sin(\pi z)(f(y)-f(x)),\,5+0.5\left(B^2{}_x+B^2{}_y+B^2{}_z\right)\right]^T$$

$$f(u)=e^{-\pi(u+1)}$$

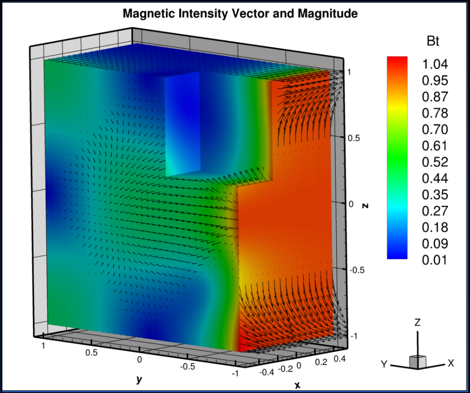

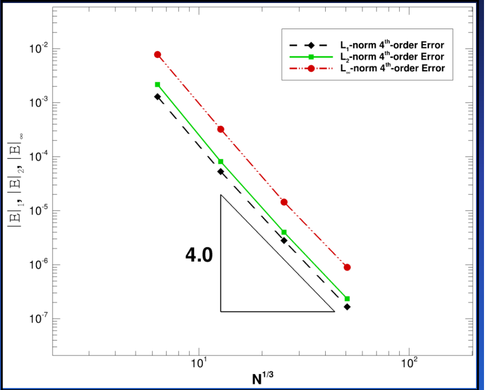

Predicted $\|\vec{B}\|$ field obtained using the **4th-order CENO** scheme with GLM-MHD on a $8\times16\times16$ mesh (left). Error norms in the predicted B_x (right).

Talk Outline

1. Governing Equations
2. Parallel Implicit Solution-Adaptive Cubed-Sphere Simulation Framework
3. Extension to High-Order Accuracy
4. Numerical Results
5. Concluding Remarks & Future Research

Concluding Remarks & Future Research

Parallel Solution-Adaptive Simulation Framework

- Developed for 3D cubed-sphere grids and space-physics flows
- Uses multi-dimensional FVM and gnomonic cubed-sphere grids
- Permits local solution-directed mesh refinement
- Extended to 4th-order accuracy using CENO + GLM-MHD
- Handles and resolves regions of strong discontinuities/shocks
- Accuracy assessment based on several test problems
- Excellent parallel performance on thousands of CPUs
- Applied to realistic solar winds for distances up to 1AU

On-Going Research

- Further investigation of the adaptive cubed-sphere algorithm in conjunction with high-order accuracy (e.g., dynamic AMR)
- Application to more complex space-physics problems (e.g., CME propagation, solar wind-magnetosphere interaction)

Acknowledgments

- This work was supported by CSA CGSM Contract No. 9F007-080157/001/ST
- Computations were performed on the GPC supercomputer at the SciNet HPC Consortium

6 Appendix

Central ENO (CENO) Reconstruction

Compromise Between Accuracy, Efficiency and Robustness

Basic Idea (Ivan & Groth, 2007, 2008, 2009, 2011):

- Combine an unlimited k-exact reconstruction with a monotonicity preserving limited linear ($k=1$) scheme, both using fixed central stencils
- Hybrid method: use a smoothness indicator to switch between the two reconstruction procedures

Note: Hybrid ENO on fixed stencil explored in 1D by Harten & Chakravarthy, 1991

Advantages of CENO Reconstruction:

- Provides **ENO-like accuracy** in smooth regions & strictly ensures **monotonicity** near discontinuities
- Always uses the **same central stencil**, avoids complexities of ENO and WENO schemes (i.e., multiple and possibly poorly conditioned stencils)
- Readily extendable to multiple dimensions & variables, unstructured mesh
- Identifies regions of **under-resolved** and **non-smooth data** (may be useful for mesh adaptation)

Central ENO (CENO) Reconstruction

Compromise Between Accuracy, Efficiency and Robustness

Basic Idea (Ivan & Groth, 2007, 2008, 2009, 2011):

- Combine an unlimited k-exact reconstruction with a monotonicity preserving limited linear ($k=1$) scheme, both using fixed central stencils
- Hybrid method: use a smoothness indicator to switch between the two reconstruction procedures

Note: Hybrid ENO on fixed stencil explored in 1D by Harten & Chakravarthy, 1991

Disadvantages of CENO Reconstruction:

- Loss of uniform accuracy (not, in the strict sense, an ENO scheme)
- Requires two solution reconstructions for non-smooth stencils

Determination of Smoothness Indicator in 3D

- Step 1: Calculate α (exploit the assumption of valid Taylor series expansion in the neighbourhood)

$$\alpha = 1 - \frac{\sum_{\gamma}\sum_{\delta}\sum_{\zeta}\left(u^k_{\gamma,\delta,\zeta}(\vec{\bar{r}}_{\gamma,\delta,\zeta}) - u^k_{i,j,\kappa}(\vec{\bar{r}}_{\gamma,\delta,\zeta})\right)^2}{\sum_{\gamma}\sum_{\delta}\sum_{\zeta}\left(u^k_{\gamma,\delta,\zeta}(\vec{\bar{r}}_{\gamma,\delta,\zeta}) - \bar{u}_{i,j,\kappa}\right)^2}$$

- Step 2: Evaluate $\mathcal{S}$ (inspired by the definition of multiple-correlation coefficients, Lawson, 1974)

$$\mathcal{S} = \frac{\alpha}{\max\left((1-\alpha), \epsilon\right)} \frac{(SOS - DOF)}{(DOF - 1)}$$

SOS : Size of Stencil; DOF : Degrees of Freedom; $\epsilon = 10^{-8}$

- Step 3: Compare to a pass/no-pass cutoff value $\mathcal{S}_c$
  - if $\mathcal{S} > \mathcal{S}_c \Rightarrow$ smooth/fully-resolved solution
  - if $\mathcal{S} < \mathcal{S}_c \Rightarrow$ non-smooth/discontinuous solution
  - $1000 \lesssim \mathcal{S}_c \lesssim 5000$ (determined from numerical experiments)

Behaviour of the Smoothness Indicator: $f(\alpha) = \dfrac{\alpha}{1-\alpha}$

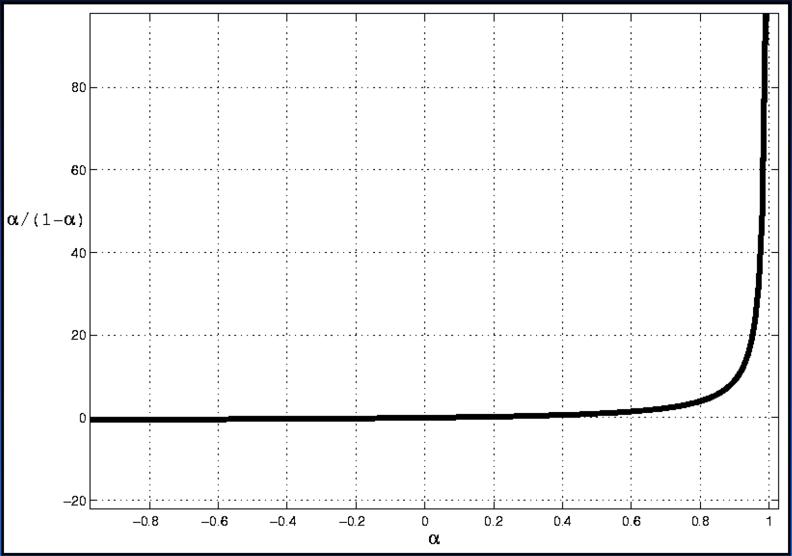

Numerical Results

Transonic Wind on Fixed Mesh

$R_i = 1$, $R_o = 10$, $GM_* = 14$, **Inflow:** $\rho = 5$, $p = 23$

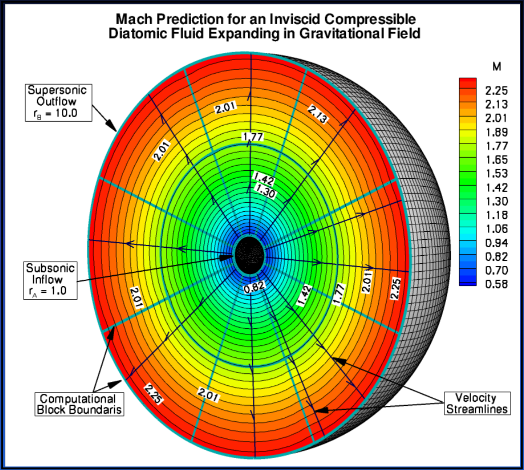

Predicted Mach number distribution obtained on a uniform mesh with 1,228,800 total cells and 128 cells in the radial direction

Numerical Results

Transonic Wind on Fixed Mesh $R_i = 1$, $R_o = 10$, $GM_* = 14$, **Inflow:** $\rho = 5$, $p = 23$

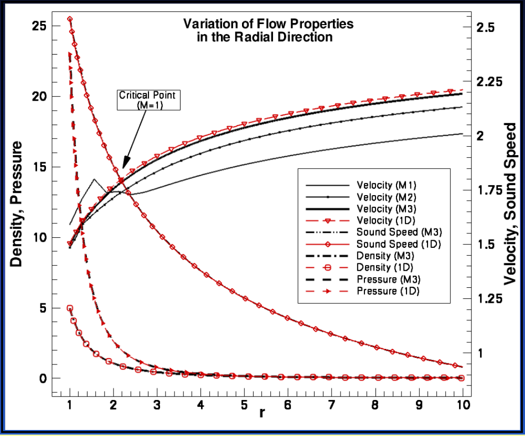

Comparison of flow properties along X-axis for M1 (19,200), M2 (153,600) and M3 (1,228,800) meshes relative to a 1D "exact solution" obtained with Newton Critical Point (NCP) method (De Sterck *et. al.* 2009).

Numerical Results

Supersonic Flow Past a Sphere

$M_\infty = 2.0$, $R_i = 1$, $R_o = 32$, $GM_* = 0$

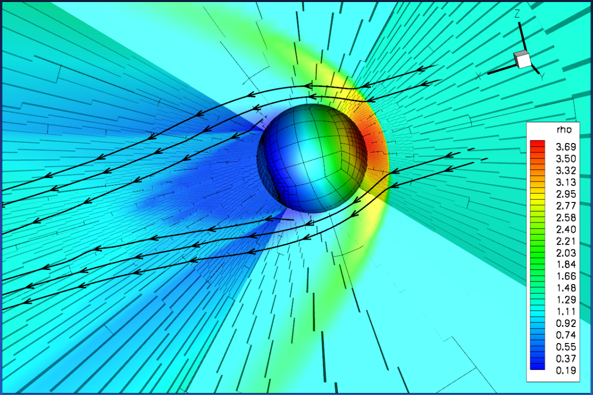

Predicted density distribution on the final refined AMR mesh with 10,835 blocks and 8,321,280 computational cells (7 levels of refinement, $\eta = 0.993$)

Numerical Results in 3D

Solution to Manufactured Problem $R_i = 2$, $R_o = 3.5$, $M_{cf} > 1$ **everywhere**

$$\mathbf{U}(x,y,z) = \left[\; r^{-\frac{5}{2}},\;\; \frac{x}{\sqrt{r}},\;\; \frac{y}{\sqrt{r}},\;\; \frac{z}{\sqrt{r}} + \kappa r^{\frac{5}{2}},\;\; \frac{x}{r^3},\;\; \frac{y}{r^3},\;\; \frac{z}{r^3} + \kappa,\;\; r^{-\frac{5}{2}} \;\right]^T, \quad \kappa = 0.017$$

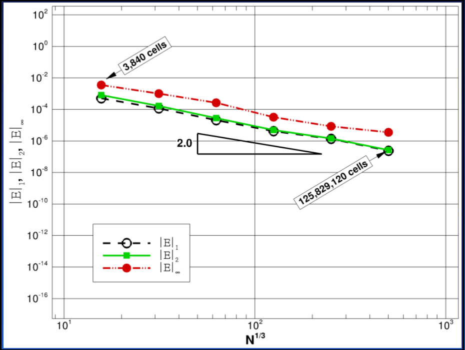

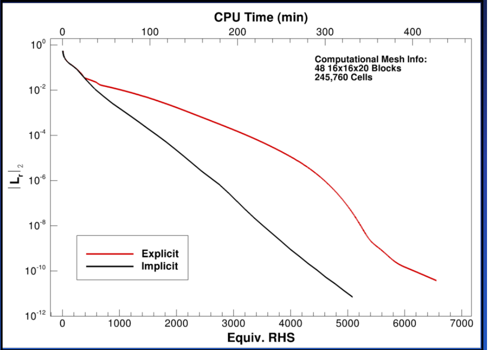

Error norms in the predicted solution density (left). Comparison of explicit and NKS implicit algorithms for the number of equivalent residual evaluations and the computational time on Intel Xeon E5540 (right).

Numerical Results in 3D

Magnetically Dominated Bow Shock

$R_i = 1,\ R_o = 8,\ M_{Ax} = 1.49,\ \theta_{vB} = 5^\circ$

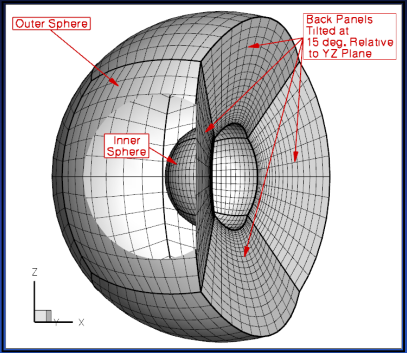

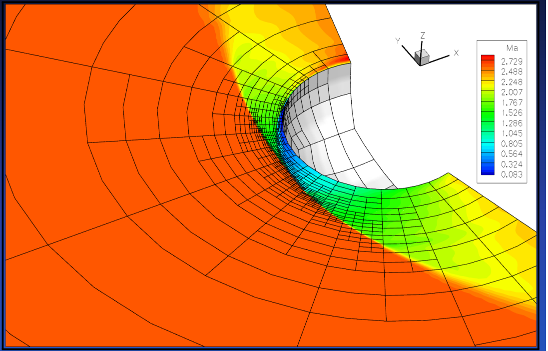

Cubed-sphere grid formed by only five root blocks (left). Predicted acoustic Mach number distribution in the (x,y) plane after 7 refinement levels and with 22,693 blocks and 14,523,520 computational cells (right).